New Series of Oxalato-Gallophosphate Structures Containing Transition Metal Centers

Wen-Ming Chang and Sue-Lein Wang*

Department of Chemistry, National Tsing Hua University, Hsinchu, Taiwan

Received April 8, 2004. Revised Manuscript Received August 23, 2004

Five organic−inorganic hybrid mixed-metal oxalatophosphates, $(C_3H_{12}N_2)_2[(VO)_2(ox)Ga_2(PO_4)_4]$ (**1**), $(C_{10}H_{28}N_4)[(VO)_2(ox)Ga_2(PO_4)_4]\cdot 2H_2O$ (**2**), $(C_7H_{21}N_3)_{0.5}(H_3O)[Mn(H_2O)_2Ga_4F_2(ox)(PO_4)_4]\cdot 4H_2O$ (**3**), $(C_5H_{14}N_2)[Mn(H_2O)_2Ga_4F_2(ox)(PO_4)_4]\cdot 3H_2O$ (**4**), and $(C_4H_{16}N_3)[MnGa_2(ox)_2(HPO_4)_2(PO_4)]$ (**5**) (ox = $C_2O_4^{2-}$), with varied framework topologies, have been synthesized under mild hydrothermal conditions and characterized by single-crystal X-ray diffraction, magnetic susceptibility, and TG analysis. They provide foremost examples of organic−metallophosphate hybrid frameworks that contain hetero metal centers, owing to which the structures of **1**−**5** are able to be indexed into a series. The vanadium compounds **1** and **2** are layered, whereas the manganese compounds **3**, **4**, and **5**, compositionally and structurally related to **1** or **2**, are 3D materials. The oxalate anion can act as a bis-bidentate ligand in all five compounds as well as a monobidentate ligand in **5**. Besides homo bioctahedral units of $M'_2(ox)O_6$ (M′ = (VO) for **1** and **2**, (GaF) for **3** and **4**), we observe the first hetero chelating $MnGa(ox)O_8$ unit, formed of an unusual $Mn^{[6p]}O_6$ trigonal prism and a GaO_6 octahedron, and unique trimeric polyhedral $Mn(H_2O)_2(GaF)_2O_{12}$ and $MnGa_2O_{16}$ units. The fundamental frameworks for **1**−**5** effectively display a series that is constructed from a substructure of 1D or 2D plus a four-ring linker and/or Mn^{2+} ions into 2D or 3D structures. The hetero metals have imposed magnetic property to the Ga(ox)PO lattices and led to the first well-defined M−X−Ga (X = O, F) bonds ever observed in the metal phosphate chemistry.

Introduction

The synthesis of organic−inorganic hybrid materials by incorporating appropriate organic ligands into the frameworks of inorganic oxides has been the subject of intense research.[1−5] The advantages of using multidentate organic components can be realized by the enhancement in the flexibility of the structure through their coordinating propensities and geometries. One class of organic−inorganic hybrid frameworks is based on oxalate and phosphate in which the metal centers are coordinated by both types of ligands. Among the various oxalatophosphates of Al,[6] Ga,[7] In,[8] Sn,[9] V,[10] Mn,[11] Fe,[12] and Zn,[13] the gallium system appears rather interesting for its unusual characteristics. For example, the Ga−O polyhedra in four-, five-, and six-coordination occur in chorus in $[Ga_5(OH)_2(C_{10}H_9N_2)(ox)(PO_4)_4]\cdot 2H_2O$[14] (ox = $C_2O_4^{2-}$), and the foremost chiral structure in the oxalatophosphate system, $(R\text{-}C_5H_{14}N_2)_2[Ga_4(ox)(H_2PO_4)_2(PO_4)_4]\cdot 2H_2O$,[15] is a gallium compound. Moreover, in comparison with transition metals, formerly reported organic gallium oxalatophosphates are much fewer, merely covering two 3D and three 2D structures.[7] After the effectual preparation of NTHU-1,[16] a GaPO structure with 24-ring channels, we have also attempted to explore the possibility of extending the channel size in the Ga/ox/P/O system. One of our approaches is to incorporate transition metals into the system to create new structures with new properties. It has successfully resulted in two layered oxalato−vanadyl(IV) gallophosphates, $(C_3H_{12}N_2)_2[(VO)_2(ox)Ga_2(PO_4)_4]$ (**1**) and $(C_{10}H_{28}N_4)[(VO)_2(ox)\ Ga_2(PO_4)_4]\cdot 2H_2O$ (**2**), and three Mn(II)-containing 3D materials, $(C_7H_{21}N_3)_{0.5}(H_3O)[Mn(H_2O)_2Ga_4F_2(ox)(PO_4)_4]\cdot 4H_2O$ (**3**), $(C_5H_{14}N_2)[Mn(H_2O)_2Ga_4F_2(ox)(PO_4)_4]\cdot 3H_2O$ (**4**), and $(C_4H_{16}N_3)[MnGa_2(ox)_2(HPO_4)_2(PO_4)]$ (**5**). They represent a new series of structures which can be constructed from $_\infty[M_2'(ox)T_2]$, a substructure of 1D or 2D with M′ = VO (**1**, **2**), GaF (**3**, **4**), and $(GaMn)_{0.5}$ (**5**), T = PO_4 (**1**−**4**) and HPO_4

* To whom correspondence should be addressed. E-mail: slwang@mx.nthu.edu.tw. Fax: 886-35-711082.

(1) Noro, S. I.; Kitagawa, S.; Kondo, M.; Seki, K. *Angew. Chem., Int. Ed.* **2000**, *39*, 2081−2084, and references therein.
(2) Eddaoudi, M.; Kim, J.; Rosi, N.; Vodak, D.; Wachter, J.; O'Keeffe, M.; Yaghi, O. M. *Science* **2002**, *295*, 469−472.
(3) James, S. L. *Chem. Soc. Rev.*, **2003**, *32*, 276−288, and references therein.
(4) Rao, C. N. R.; Natarajan, S.; Vaidhyanathan, R. *Angew. Chem., Inter. Ed.* **2004**, *43*, 1466−1496, and references therein.
(5) Liao, Y. C.; Liao, F. L.; Chang, W. K.; Wang, S. L. *J. Am. Chem. Soc.* **2004**, *126*, 1320−1321, and reference therein.
(6) Rajic, N.; Logar, N. Z.; Mali, G.; Kaučič, V. *Chem. Mater.* **2003**, *15*, 1734−1738.
(7) Hung, L. C.; Kao, H. M.; Lii, K. H. *Chem. Mater.* **2000**, *12*, 2411−2417.
(8) Huang, Y. F.; Lii, K. H. *J. Chem. Soc., Dalton Trans.* **1998**, 4085−4086.
(9) Natarajan, S. *J. Solid State Chem.* **1998**, *139*, 200−203.
(10) Tsai, Y. M.; Wang, S. L.; Huang, C. H.; Lii, K. H. *Inorg. Chem.* **1999**, *38*, 4183−4187.
(11) Lethbridge, Z. A. D.; Smith, M. J.; Tiwary, S. K.; Harrison, A.; Lightfoot, P. *Inorg. Chem.* **2004**, *43*, 11−13.
(12) Jiang, Y. C.; Wang, S. L.; Lii, K. H. *Chem. Mater.* **2003**, *15*, 1633−1638.
(13) Neeraj, S.; Natarajan, S.; Rao, C. N. R. *J. Chem. Soc., Dalton Trans.* **2001**, 289−291.
(14) Chen, C. Y.; Chu, P. P.; Lii, K. H. *J. Chem. Soc., Chem. Commun.* **1999**, 1473−1474.
(15) Lii, K. H.; Chen, C. Y. *Inorg. Chem.* **2000**, *39*, 3374−3378.
(16) Lin, C. H.; Wang, S. L.; Lii K. H. *J. Am. Chem. Soc.* **2001**, *123*, 4649−4650.

10.1021/cm049411v CCC: $30.25
Published on Web 12/07/2004

Table 1. Crystallographic Data for $(C_3H_{12}N_2)_2[(VO)_2(ox)Ga_2(PO_4)_4]$ (1), $(C_{10}H_{28}N_4)[(VO)_2(ox)Ga_2(PO_4)_4]\cdot 2H_2O$ (2), $(C_7H_{21}N_3)_{0.5}(H_3O)[Mn(H_2O)_2Ga_4F_2(ox)(PO_4)_4]\cdot 4H_2O$ (3), $(C_5H_{14}N_2)[Mn(H_2O)_2Ga_4F_2(ox)(PO_4)_4]\cdot 3H_2O$ (4) and $(C_4H_{16}N_3)[MnGa_2(ox)_2(HPO_4)_2(PO_4)]$ (5) (ox = $C_2O_4^{2-}$)

	1	2	3	4	5
chemical formula	$C_8H_{24}Ga_2N_4O_{22}P_4V_2$	$C_{12}H_{32}Ga_2N_4O_{24}P_4V_2$	$C_{5.5}H_{25.5}F_2Ga_4MnN_{1.5}O_{27}P_4$	$C_7H_{24}F_2Ga_4MnN_2O_{25}P_4$	$C_8H_{18}Ga_2MnN_3O_{20}P_3$
fw	893.52	981.62	1040.47	1031.98	763.54
a/Å	15.8224(7)	8.2932(4)	18.952(1)	8.1452(8)	9.5286(8)
b/Å	9.0385(4)	9.0002(5)	15.964(1)	8.9029(9)	10.1451(8)
c/Å	17.4504(8)	10.1814(5)	9.0028(6)	10.445(1)	12.579(1)
α/deg		82.415(1)		111.437(2)	86.429(1)
β/deg		81.080(1)	97.927(1)	103.734(2)	69.606(1)
γ/deg		78.572(1)		102.096(2)	62.338(1)
V/Å^3	2495.5(1)	731.83(6)	2697.9(3)	647.0(1)	1002.2(1)
Z	4	1	4	1	2
space group	*Pbca* (No. 61)	$P\bar{1}$ (No. 2)	*C*2/*c* (No. 15)	$P\bar{1}$ (No. 2)	$P\bar{1}$ (No. 2)
T/°C	20	20	−173	20	22
λ(Mo Kα)/Å	0.71073	0.71073	0.71073	0.71073	0.71073
ρ_{calcd}/g·cm^{-3}	2.378	2.227	2.562	2.648	2.530
μ(Mo Kα)/cm^{-1}	32.3	27.7	47.7	49.6	36.4
R_1[a]	0.0310	0.0421	0.0479	0.0515	0.0361
wR_2[b]	0.0842	0.1164	0.1567	0.1452	0.0893

[a] $R_1 = ||F_o| - |F_c||/|F_o|$ for $F_o > 4\sigma(F_o)$. [b] w$R_2 = 1/[\sigma^2(F_o^2) + (aP)^2 + bP]$, $P = [\mathrm{Max}(F_o) + 2(F_c)^2]/3$, where $a/b = 0.0543/0.0$ for **1**, 0.0676/0.0 for **2**, 0.0999/38.09 for **3**, 0.0948/3.14 for **4**, and 0.0274/3.99 for **5**.

(**5**), plus 4-rings linkers ([GaT] (**1**−**4**) and [GaT(ox)] (**5**). Other than metal oxalates, no mixed-metal oxalatophosphate has been documented till date. Herein, we report the syntheses, crystal structures, structural relationship along with amine-template and heteroatom effects, magnetic property, and thermal stability of the first series of organic−inorganic hybrid mixed-metal oxalatophosphates.

Experimental Section

Synthesis and Initial Characterization. Compounds **1**−**5** were synthesized via typical hydrothermal reactions[17] with different organic amines as structure directing reagents. The other chemicals included $Ga(NO_3)_3\cdot 9H_2O$, $H_2C_2O_4\cdot 2H_2O$, 85% H_3PO_4, KVO_3, and $MnCl_2\cdot 2H_2O$. The mole ratios of amine, Ga, V (or Mn), oxalic acid, and P were kept at 2:1:0.4:2:5 initially for all reactions. They are categorized into two groups by distinct solvent systems, group **I** for pure water (1.5 < pH < 2.3), and group **II** for water/*n*-butanol/HF in the mole ratio of 214:18:1 (2.1 < pH < 3.16). In the group **I** reactions, the use of 1,3-diaminopropane (dap) and diethylenetriamine (dien) separately resulted in green crystals of **1** and transparent crystals of **5**. Optimum conditions can be achieved by reducing the amount of H_3PO_4 from 5 to 3 mmol plus, increasing the amount of KVO_3 from 0.4 to 0.6 mmol for **1** (major product), or adding 1 mmol of tetrabutylammonium chloride for **5** (single-phased product). In the group **II** reactions, 1,4-bis(3-aminopropyl)-piperazine (appip), 3,3′-diamino-*n*-methyldipropylamine (damdp) and 1-(2-aminoethyl)piperazine (aepip) were employed and thereby respectively yielded green crystals of **2** and transparent crystals of **3** and **4**. Compound **2** was only a minor phase while **3** and **4** were major in each individual product. All amines remained essentially intact in the crystalline products except aepip, which cleaved into (1-methyl)piperazine (mpip) as observed in **4**.[18] All measurements (vide infra) were performed on samples of manually picked crystals. The specific amount of V, Mn, and Ga atoms determined from single-crystal structure refinements were additionally evidenced by electron probe microanalysis (EPMA). The results of elemental analyses (EA) confirmed the stoichiometry of organic amines. Found/Calcd: C, 10.47/10.75; H, 3.08/2.71; N, 6.45/6.27% for **1**; C, 6.33/6.35; H, 2.49/2.47; N, 2.15/2.02 for **3**; C, 8.07/8.15; H, 2.60/2.34; N, 2.92/2.71% for **4**; and C, 12.64/12.58; H, 2.54/2.38; N, 5.51/5.50% for **5**.

Single-Crystal Structure Analysis. Crystals with varied dimensions for **1**−**5** were selected for indexing and intensity data collection on Bruker CCD diffractometers (λ = 0.71073 Å). All intensity data were collected at room temperature and absorption and *LP* corrections were made thereupon.[19] Determination of the space groups was based on statistics of intensity distribution, systematic absences, and successful structural solutions and refinements. Initial models were solved by direct methods with the metal (Ga, V, or Mn) and P atoms disclosed first, followed by the atoms of O/F, N, and C atoms located on successive difference Fourier maps for **1**, **2**, **4**, and **5**. For **3**, however, no organic cations could be scrutinized on Fourier syntheses before low-T intensity data (re-collected at 100 K) were analyzed. Yet only fragments of the damdp molecule could be retrieved from ED maps. For **4**, the observed organic amine molecules were well confirmed by EA to be mpip, a product of the reactant aepip. Hydrogen atoms of coordination waters (**3** and **4**) and the HPO_4 group (**5**) were directly located on final difference maps. Those of the organic amines were only partially observed. The final cycles of least-squares refinement, including the atomic coordinates and anisotropic thermal parameters of all non-hydrogen atoms and fixed coordinates and isotroptic thermal parameters for observed H atoms, converged at R1 = 0.0310, S = 1.05 for **1**; R1 = 0.0421, S = 1.08 for **2**; R1 = 0.0479, S = 1.15 for **3**; R1 = 0.0515, S = 1.10 for **4**; and R1 = 0.0361, S = 1.11 for **5**. Neutral-atom scattering factors were used for all the atoms. Anomalous dispersion and secondary extinction corrections were applied. All calculations were performed by using the PC version of the SHELXTL program package. Crystallographic data are listed in Table 1 and selected bond distances are reported in Table 2.

(17) The reaction mixture was placed in a Teflon-lined Parr bomb (60% filling) and heated at 160 °C for **1**−**4** and 170 °C for **5** for 3 days. The resulting products were green crystals for **1** and **2** and pale pink crystals for **3**, **4**, and **5**.

(18) Compound **4** was first prepared with pip, resulting in a clear structure with ordered template but a yield too poor for further characterizations. Substituting pip with aepip resulted also in structure **4**, only that the template molecules, having broken into mpips during reaction, are disordered in the channels and that the yield is sufficient to our experimental need.

(19) Bruker Analytical X-ray System. *SAINT+ programs*, Release Version 6.02, 1999.

Table 2. Selected Bond Lengths (Å) for the Anionic Frameworks of 1−5

1		**2**		**3**		**4**	
Ga(1)−O(1)	1.816(2)	Ga(1)−O(1)	1.820(3)	Ga(1)−O(2)	1.820(4)	Ga(1)−O(1)	1.811(4)
Ga(1)−O(3)	1.819(2)	Ga(1)−O(2)	1.808(3)	Ga(1)−O(3)	1.832(4)	Ga(1)−O(2)	1.823(4)
Ga(1)−O(5)	1.817(2)	Ga(1)−O(6)	1.829(3)	Ga(1)−O(5)	1.831(4)	Ga(1)−O(6)	1.825(4)
Ga(1)−O(6)	1.825(2)	Ga(1)−O(7)	1.829(3)	Ga(1)−O(6)	1.830(4)	Ga(1)−O(7)	1.835(3)
$Ga-O_{ave}$ = 1.820				$Ga-O_{ave}$ = 1.825			
V(1)−O(4)	1.962(2)	V(1)−O(3)	1.956(3)	Ga(2)−O(4)	1.919(4)	Ga(2)−O(3)	1.917(4)
V(1)−O(7)	1.994(2)	V(1)−O(5)	1.950(3)	Ga(2)−O(7)	1.946(4)	Ga(2)−O(5)	1.915(4)
V(1)−O(8)	1.939(2)	V(1)−O(8)	1.972(3)	Ga(2)−O(8)^{i}	1.897(4)	Ga(2)−O(8)	1.912(4)
V(1)−O(9)	2.196(2)	V(1)−O(9)	2.163(3)	Ga(2)−O(9)	2.017(4)	Ga(2)−O(9)	2.020(4)
V(1)−O(10)	2.080(2)	V(1)−O(10)	2.077(3)	Ga(2)−O(10)	2.041(4)	Ga(2)−O(10)	2.045(4)
V(1)−O(11)	1.655(2)	V(1)−O(11)	1.696(3)	Ga(2)−F(1)	1.873(3)	Ga(2)−F(1)	1.876(3)
$V-O_{ave}$ = 1.970				$Ga-O_{ave}$ = 1.963			
P(1)−O(1)	1.552(2)	P(1)−O(1)	1.550(3)	Mn(1)−O(1)	2.116(4) (2x)	Mn(1)−O(4)	2.159(4) (2x)
P(1)−O(2)	1.507(2)	P(1)−O(2)	1.551(3)	Mn(1)−O(11)	2.238(10) (2x)	Mn(1)−O(11)	2.203(5) (2x)
P(1)−O(3)	1.553(2)	P(1)−O(3)	1.513(3)	Mn(1)−F(1)	2.131(3) (2x)	Mn(1)−F(1)	2.110(3) (2x)
P(1)−O(4)	1.507(2)	P(1)−O(4)	1.517(3)	$Mn-O_{ave}$ = 2.179		$Mn-F_{ave}$ = 2.121	
$P-O_{ave}$ = 1.532				P(1)−O(1)	1.509(4)	P(1)−O(1)	1.547(4)
P(2)−O(5)	1.533(2)	P(2)−O(5)	1.509(3)	P(1)−O(2)	1.551(4)	P(1)−O(2)	1.553(4)
P(2)−O(6)	1.549(2)	P(2)−O(6)	1.551(3)	P(1)−O(3)	1.550(4)	P(1)−O(3)	1.522(4)
P(2)−O(7)	1.517(2)	P(2)−O(7)	1.555(3)	P(1)−O(4)	1.522(4)	P(1)−O(4)	1.508(4)
P(2)−O(8)	1.515(2)	P(2)−O(8)	1.516(3)	$P-O_{ave}$ = 1.533			
$P-O_{ave}$ = 1.531				P(2)−O(5)	1.540(4)	P(2)−O(5)	1.510(4)
C(1)−C(1)	1.534(6)	C(1)−C(1)	1.552(9)	P(2)−O(6)	1.549(4)	P(2)−O(6)	1.535(4)
C(1)−O(9)	1.244(4) (2x)	C(1)−O(9)	1.256(5) (2x)	P(2)−O(7)	1.532(4)	P(2)−O(7)	1.544(4)
C(1)−O(10)	1.258(3) (2x)	C(1)−O(10)	1.242(5) (2x)	P(2)−O(8)	1.512(4)	P(2)−O(8)	1.512(4)
$C-O_{ave}$ = 1.250				$P-O_{ave}$ = 1.529			
				C(1)−C(1)	1.56(1)	C(1)−C(1)	1.54(1)
				C(1)−O(9)	1.258(6) (2x)	C(1)−O(9)	1.263(6) (2x)
				C(1)−O(10)	1.253(6) (2x)	C(1)−O(10)	1.255(6) (2x)
				$C-O_{ave}$ = 1.258		$C-C_{ave}$ = 1.55	

5			
Ga(1)−O(1)	1.920(3)	Ga(1)−O(9)	1.922(3)
Ga(1)−O(2)	1.928(3)	Ga(1)−O(15)	2.007(3)
Ga(1)−O(7)	2.021(3)	Ga(1)−O(16)	2.036(3)
$Ga-O_{ave}$ = 1.972			
Ga(2)−O(3)	1.956(3)	Ga(2)−O(10)	1.914(3)
Ga(2)−O(5)	1.936(3)	Ga(2)−O(13)	2.048(3)
Ga(2)−O(6)	1.995(3)	Ga(2)−O(14)	2.032(3)
$Ga-O_{ave}$ = 1.980			
Mn(1)−O(6)	2.466(3)	Mn(1)−O(12)	2.103(3)
Mn(1)−O(7)	2.181(3)	Mn(1)−O(17)	2.227(3)
Mn(1)−O(11)	2.078(3)	Mn(1)−O(18)	2.198(3)
$Mn-O_{ave}$ = 2.209			
P(1)−O(1)	1.515(3)	P(1)−O(2)	1.530(3)
P(1)−O(3)	1.527(3)	P(1)−O(4)	1.587(3)
$P-O_{ave}$ = 1.540			
P(2)−O(5)	1.507(3)	P(2)−O(6)	1.532(3)
P(2)−O(7)	1.544(3)	P(2)−O(8)	1.570(3)
$P-O_{ave}$ = 1.538			
P(3)−O(9)	1.538(3)	P(3)−O(10)	1.553(3)
P(3)−O(11)	1.525(3)	P(3)−O(12)	1.533(3)
$P-O_{ave}$ = 1.537			
C(1)−C(2)	1.553(6)	C(3)−C(4)	1.540(6)
C(1)−O(16)	1.262(5)	C(3)−O(13)	1.262(5)
C(1)−O(19)	1.232(5)	C(3)−O(18)	1.237(5)
C(2)−O(15)	1.274(5)	C(4)−O(14)	1.268(5)
C(2)−O(20)	1.236(5)	C(4)−O(17)	1.244(5)
$C-O_{ave}$ = 1.252		$C-C_{ave}$ = 1.547	

Thermal Analysis. Thermogravimetric analyses (TGA), using a Perkin-Elmer TGA-7 or a LABSYS thermal analyzer, were performed on powder samples of **1** (5.85 mg), **3** (6.62 mg), **4** (7.42 mg) and **5** (20.59 mg) under flowing nitrogen at a heating rate of 10 °C min^{-1}. The TG curves (see Supporting Information) clearly indicate that the two nonhydrated compounds **1** and **5** could be thermally stable up to 300 °C and the two hydrates **3** and **4** would immediately began to lose weight upon heating. For all four compounds the removal of organic amines and oxalate groups gave unresolved TG curves. The total observed weight loss, 27.5% for **1** and 36.2% for **5**, can be compared with those calculated, 26.86% from 2dap + 2CO + $2H_2O$ for **1** and 36.27% from dien + $2.5H_2O$ + 3CO + CO_2 for **5**. For compounds **3** and **4** the observed weight loss up to ∼550 °C should correspond to the removal of lattice water and organic amines (20.82% from 0.5damdp + 8 H_2O for **3** and 20.38% from 1mpip + $6H_2O$ for **4**). Similar to **5**, the oxlate groups in **3** and **4** were not completely removed on heating to 1000 °C.

Magnetic Susceptibility Measurements. Powder samples of **1** (11.2 mg), **3** (27.9 mg), **4** (33.5 mg), and **5** (28.0 mg) were used to collect variable temperature magnetic susceptibility $\chi(T)$ data from 2 to 300 K in a magnetic field of 5 kG after zero-field cooling using a Quantum Design SQUID magnetometer. Correction for diamagnetism was made according to Selwood.[20] The data are fitted

(20) Selwood, P. W. *Magnetochemistry*; Interscience: New York, 1956.

Table 3. General Formulas for the Anionic Framework, Weiss Constants, the Effective Magnetic Moments Derived from Magnetic Susceptibility Data, and the Nearest Metal to Metal Distance

	anionic framework					
	general formula	M′	T	Θ (K)	μ_{eff} (B. M.)	M···M* (Å)
1	$[M'_2(ox)T_2(4R_t)]^{2-}$	VO	PO_4	−4.06	1.54	5.579
2	$[M'_2(ox)T_2(4R_t)]^{4-}$	VO	PO_4			5.540
3	$[Mn(H_2O)_2\ M'_2(ox)T_2(4R_t)]^{2-}$	GaF	PO_4	−1.12	5.92	6.020
4	$[Mn(H_2O)_2M'_2(ox)T_2(4R_t)]^{2-}$	GaF	PO_4	−0.47	5.92	8.145
5	$[M'_2(ox)T_2\ (4R_o)]^{3-}$	$(MnGa)_{0.5}$	HPO_4	−1.98	5.95	4.734

by a Curie−Weiss equation, $\chi_M = C/(T - \theta)$, which reveals antiferromagnetism at low T for all four compounds. All fitting curves are provided in the Supporting Information. The resulting Weiss constants and effective magnetic moments together with the distances between magnetic centers are given in Table 3.

Results and Discussion

Structure Description and Relationship. Both **1** and **2** are constructed from VO_6 octahedron, ox group, GaO_4, and PO_4 tetrahedra to form two-dimensional structures with the same layer composition but distinct topologies. There exist two common secondary building units: a bioctahedral $[(VO)_2(ox)O_6]$ cluster (SBU_V), formed of two VO_6 and a bis-bidentated ox ligand (Figure 1), and a tetrahedral four-ring $[GaPO_4]$ unit ($4R_t$), formed of GaO_4 and $P(1)O_4$ tetrahedra. As depicted in Figure 2, each SBU_V, via four tetrahedra ($P(2)O_4$), can connect to another four SBU_V to give an infinite $^2_\infty[(VO)_2(ox)(PO_4)_2]$ net (*net I*), or link to another two to give an infinite $^1_\infty[(VO)_2(ox)(PO_4)_2]$ chain (*chain I*). The layers in **1**, **L1**, are essentially a collection of *net I* plus $4R_t$ lodging in the pores within the nets, whereas the layers in **2**,[21] **L2**, are built up with *chains I* interlinked by $4R_t$. As shown in Figure 3, two different forms of layers, respectively wavelike and flat, are resulted with different spans: 7.911 Å for **1** and 8.293 Å for **2**. Moreover, the dissimilar interlayer amine cations (two arrays of dap molecules in **1** and one array of appip in **2**) have made different layer separations (8.725 vs 10.029 Å).

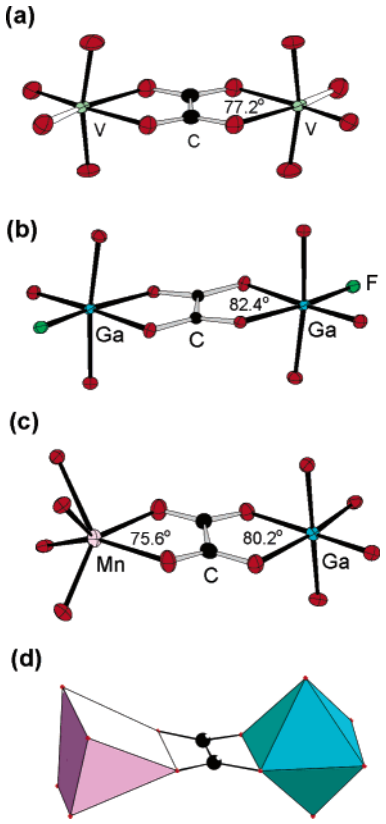

Figure 1. Common secondary building units: (a) bioctahedral $[(VO)_2(ox)O_6]$ unit (SBU_v) in **1** and **2**; (b) bioctahedral $[(GaF)_2(ox)O_6]$ cluster (SBU_{Ga}) in **3** and **4**; (c) the hetero chelating $MnGa(ox)O_8$ unit (SBU_{Mn}) in **5**; (d) polyhedral representation of SBU_{Mn} showing an unusual $Mn^{[6p]}O_6$ trigonal prism (pink) and a GaO_6 octahedron (cyan). Oxalate biting angles on metal sites are showing in (a), (b) and (c) where the two metal centers are apart by 5.56 Å in SBU_v, 5.31 Å in SBU_{Ga}, and 5.53 Å in SBU_{Mn}.

The frameworks of **3** and **4** (Figure 3) can be described by constructing from the respective layers **L1** and **L2**, which are propped up into three-dimensional with Mn^{2+} ions, the 3D linker. The difference lies in the substitution of intralayer octahedral cores $[VO]^{2+}$ in SBU_V with $[GaF]^{2+}$ (SBU_{Ga}) (Figure 1b). The connections between neighboring layers are made through $MnO_2F_2(H_2O)_2$, corner-shared with GaO_5F octahedral within adjacent layers, therefore forming unique trimeric octahedral $Mn(H_2O)_2(GaF)_2O_{12}$ clusters. The linear-shaped trimers have perpendicular 2-fold symmetry in **3**, while there is inversion in **4** (Figure 4). Another difference lies in the configuration of $MnO_2F_2(H_2O)_2$ octahedra, where the two water ligands are in cis positions in **3** but trans in **4**. Between adjacent layers the trimers embrace straight channels, two types (8R and 12R) in **3** and one type (10R) in **4** (see Figure 5). The 8R channel contains no counter species whereas the ones with 12R and 10R apertures are filled with disordered amine cations and lattice H_2O. The framework topology of **3** is analogous to $[Ga_5(OH)_2(C_{10}H_9N_2)(ox)(PO_4)_4]\cdot 2H_2O$,[14] only that the 3D linkers $MnO_2F_2(H_2O)_2$ octahedra are replaced by GaO_4N square pyramids, the 8R channels are occupied by H_2O, and the amine cations are in ancillary ligation to Ga^{3+} centers.

Compound **5** is also a Mn^{2+}-containing 3D structure[22] built up with MnO_6, GaO_6, ox groups, PO_4, and HPO_4, but no GaO_4 tetrahedra. The Mn and half of the Ga centers, Ga(2), are linked to the same ox group to form an unprecedented hetero $MnGa(ox)O_8$ cluster (SBU_{Mn}) (Figure 1c). The other half of the Ga centers, Ga(1), are coordinated by a monobidentate ox group and link to $HP(1)O_4$ groups to form an octahedral−tetrahedral four-ring $[Ga(ox)HPO_4]$ unit ($4R_o$). Each SBU_{Mn} connects to another four SBU_{Mn} via four tetrahedra ($2HPO_4$ and $2PO_4$) to generate an infinite $^2_\infty[Mn(ox)Ga(PO_4)(HPO_4)]$ net (*net II*, Figure 6). Two *net II*

(21) The layers in **2**, although differing in composition and symmetry, somewhat resemble that of $(R\text{-}C_5H_{14}N_2)_2[Ga_4(ox)(H_2PO_4)_2\ (PO_4)_4]\cdot 2H_2O$ (ref 15).

(22) The Fe^{2+} and Fe^{3+} ion sites in $(H_3deta)[Fe_3(ox)_2(HPO_4)_2(PO_4)]$[12] can be respectively replaced by Mn^{2+} and Ga^{3+} to become **5**. The greatest difference lies in the five-coordinated Fe^{2+} and six-coordinated Mn^{2+} sites.

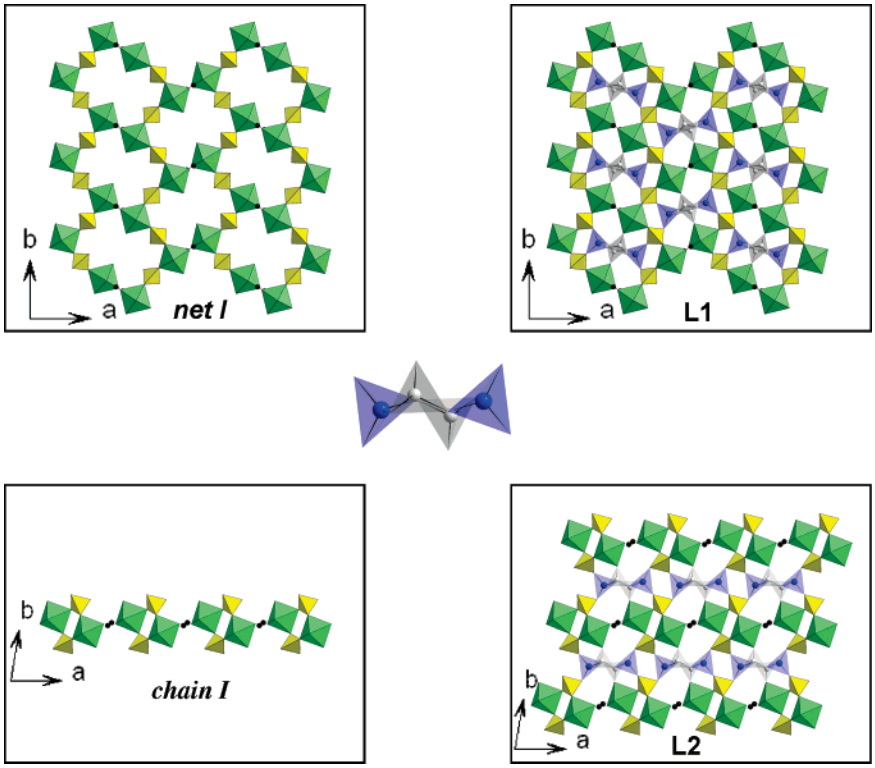

Figure 2. Polyhedral representations of substructures, linker, and layers in **1** and **2**. Left: net *I* or chain *I* built up with SBU_v (green) and $P(2)O_4$ tetrahedra (yellow). Middle: the tetrahedral four-ring [$GaPO_4$] linker formed of GaO_4 (blue) and $P(1)O_4$ (gray). Right: layers **L1** (or **L2**) are constructed from net *I* (or chain *I*) and $4R_t$.

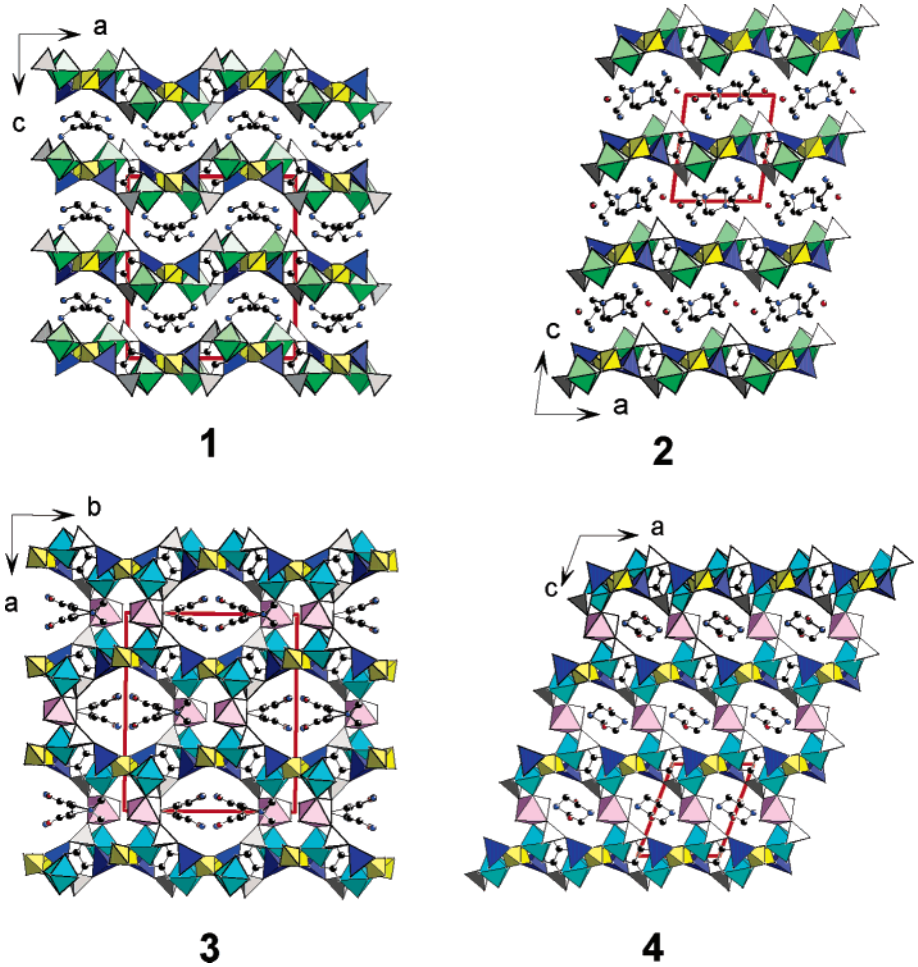

Figure 3. Perspective views of the structures of **1**−**4**. The 2D structure of **1** is converted into the 3D structure of **3** by the presence of Mn^{2+} ion (pink octahedra) as the structure linker. The same relationship exists between **2** and **4**. In these representations, the octahedra VO_6 are green, MnO_6 are pink, and GaO_6 are cyan, and tetrahedra GaO_4 are blue, $P(1)O_4$ are gray, and $P(2)O_4$ are yellow. Ox groups, amine cations, and water molecules are in ball-and-stick model (C black, N blue, and O red). H atoms are omitted for clarity.

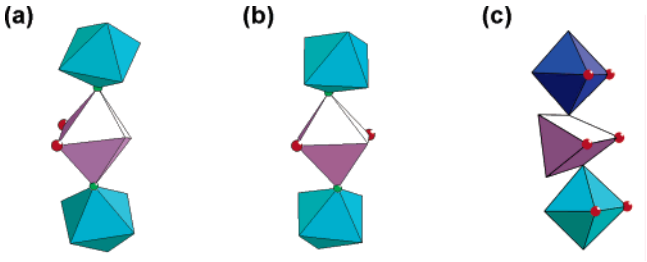

Figure 4. Unique trimeric clusters in (a) **3**; (b) **4**; and (c) **5**. Red circles in (a) and (b) represent water oxygens, in (c) oxlate oxygens. Green circles in (a) and (b) are F sites. ∠Ga−F−Mn = 134.3° in (a) and 133.5° in (b), and ∠Ga−O−Mn = 122.6° and 124.2° in (c).

can fuse together via the common vertexes from $HP(2)O_4$ and $P(3)O_4$ to create a doublet which keeps the same composition as a singlet. As depicted in Figure 7, the 3D network of **5** is constructed from the doublets of net *II* and $4R_o$. It is interesting to note that the coordination geometry for Mn^{2+} ions in **5** is trigonal prism ([6p]) which scarcely occurs in phosphate chemistry. Furthermore, each $Mn^{[6p]}O_6$ unit shares a triangle edge with two GaO_6 octahedra, forming a trimeric $MnGa_2O_{16}$ unit (Figure 4) and leading to the first well-defined M−O−Ga bond ever observed in metal phosphate structures.

From the structure point of view, **1**−**5** share three features. First, in all five compounds, the ox groups chelate all octahedral metal centers and the MO_6 polyhedra can be paired via a bridging ox group into clusters of SUB_v, SUB_{Ga}, and SUB_{Mn}. Second, they all possess an anionic substructure of $_\infty[M_2'(ox)T_2]^{4-}$ which may be 1D (*chain I*) or 2D (*net I* and *net II*) with M′ = VO, GaF, $(GaMn)_{0.5}$, and T = phosphate tetrahedron. Third, they all have 4R units of [GaT] ($4R_t$ or $4R_o$), acting as linkers to convert a 1D substructure into 2D or a 2D substructure into 3D. General formulas for **1**−**5** are given in Table 3.

Amine-Template and Hetero-Atom Effects. Among the series, five different framework topologies are resulted from dissimilar amine molecules. Though incorporating with V and Mn, a particular amine only responds to either of the metals, working as the structure-directing reagents. For example, the replacement of V with Mn in the preparation of **1** and **5** in the group **I** reactions fails to produce any equivalence. Similarly, no corresponding products can be achieved via substituting Mn for V in the synthesis of **2**−**4** in the group **II** reactions, where the fluoride ion may play an important role as well. The vanadium compounds **1** and **2** are two-dimensional and the layers cannot be connected into 3D networks due to the terminal V═O groups pointing into the interlayer space. In comparison, the Mn compounds **3**−**5** are 3D structures where nanosized channels are observed (Figure 5). Based on structure refinements, amine templates in **1**, **2**, and **5** are ordered but in **3** and **4** are disordered. These results are in accordance with their TG curves where the loss of disordered amine molecules occurred at a lower temperature (**3** or **4**) than for ordered ones (**1** and **5**).

Summary

Two transition metal ions, V^{4+} and Mn^{2+}, have been successfully embedded in Ga(ox)PO frameworks and resulted in the first series of organic−inorganic hybrid mixed-metal oxalatophosphates, **1**−**5**. The hetero metals have not only imposed magnetic properties but also led to the first well-defined Mn−X−Ga (X = O and F) bonds ever observed in the metal phosphates. Owing to the presence of hetero metals the five structures are able to be indexed into a series, with a general formula $[M'_2(ox)T_2(4R)]$ for the fundamental framework, which may be 2D for **1**−**4** or 3D for **5**. We have also observed that the general formula can be extended to other metal oxalatophosphates.[12−15] The V^{4+} ions in **1** and **2**

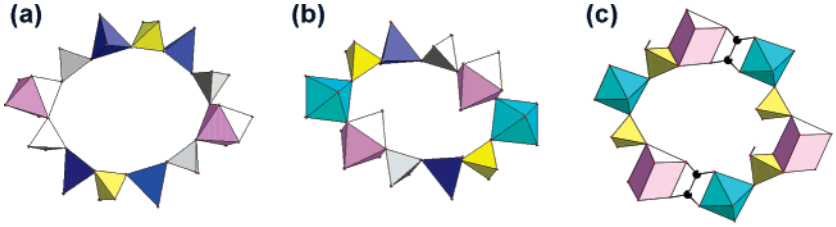

Figure 5. Channel apertures observed in **3**−**5**: (a) 12 R (1.15 nm) in **3**, (b) 10R (0.975 nm) in **4**, and (c) 10R+2ox (1.16 nm) in **5**. Values shown in parentheses are the maximum diameters (atom-to-atom distances).

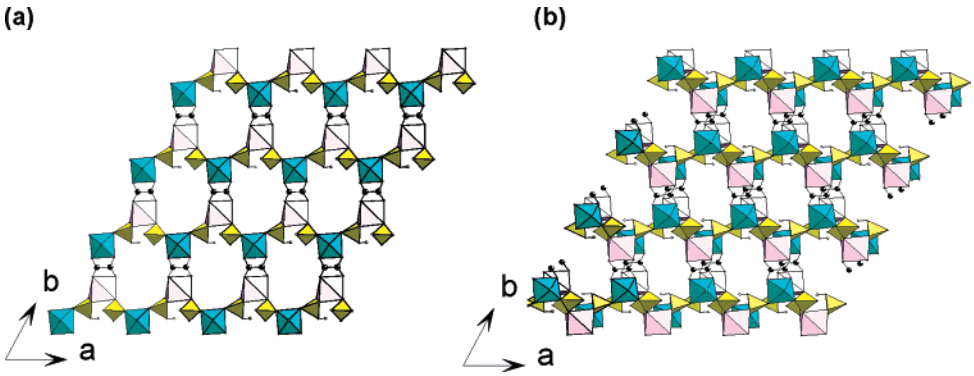

Figure 6. Section of infinite $^2_\infty[Mn(ox)Ga(PO_4)(HPO_4)]$ net in **5**, view along the *c*-axis: (a) net *II*, formed of SBU_{Mn} and tetrahedral of $HP(2)O_4$ and $P(3)O_4$; (b) a doublet of net *II*.

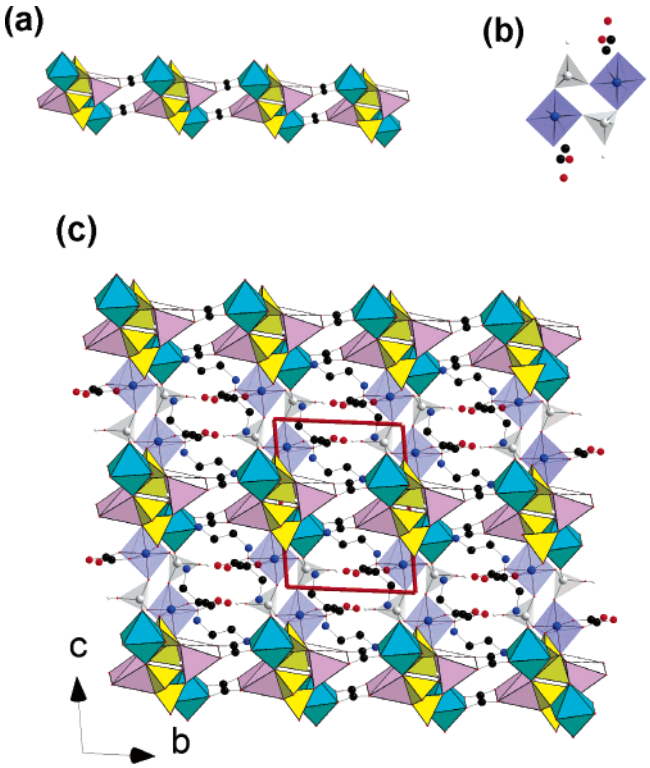

Figure 7. Construction of 3D network of **5** from 2D substructure and four-ring linker: (a) side view of the doublet of net *II*; (b) the octahedra-tetrahedra four-ring [Ga(ox)HPO_4] unit, $4R_o$; (c) a perspective view of **5** along the *a*-axis.

are paired by ox groups such as octahedral Ga^{3+} centers, and they diminish or retain structural dimensions. By contrast, the Mn^{2+} ions, which are not coordinated by ox groups, can act as a linker to convert layers (**L1** and **L2**) into 3D networks (**3** and **4**). Thus, the structure of **1** represents a unique 2D version of **3**, and **4** is a unique 3D version of **2**. In regard to **5**, the Mn^{2+} ions, chelated by ox groups, do not act as a linker for higher dimension but result in an unusual 6p geometry wherein the 3D linkers are $4R_o$ groups. In comparison with **3** and **4**, the ox-rich framework of **5** is more stable. Investigation of extra-large pore materials with better thermal stability in the mixed-metal organic−phosphate hybrid materials is in progress.

Acknowledgment. We are grateful to the National Science Council of Taiwan for support of this work (92-2113-M-007-029). W.M.C. also thanks to W. J. Tsai for assistance in magnetic study and discussions on hydrothermal synthesis.

Supporting Information Available: X-ray crystallographic information files (CIF) for **1**−**5**. TG and Magnetic susceptibility curves for **1** and **3**−**5** (pdf). This material is available free of charge via the Internet at http://pubs.acs.org.

CM049411V